PHYSICAL REVIEW B **76**, 125203 (2007)

Conduction-band dispersion relation and electron effective mass in III-V and II-VI zinc-blende semiconductors

S. Shokhovets,[1,*] O. Ambacher,[2] and G. Gobsch[1]

[1]*Institute of Physics, Ilmenau Technical University, D-98684 Ilmenau, Germany*

[2]*Institute of Micro- and Nanotechnologies, Ilmenau Technical University, D-98684 Ilmenau, Germany*

(Received 9 May 2007; revised manuscript received 19 July 2007; published 10 September 2007)

Adjusting calculated spectra of the imaginary part ε_2 of the dielectric function to experimental ones in a spectral region close to and above the fundamental absorption edge, we determined the conduction-band dispersion relation for 12 III-V and II-VI semiconductors with zinc-blende crystal structure and deduced the corresponding nonparabolicity coefficients. This yields an experimental determination of the conduction-band nonparabolicity and momentum electron effective mass as a function of the wave vector and free electron concentration. For most of the semiconductors, we present experimental data extended to electron energies between 0.6 and 2.2 eV, which are significantly higher than those achievable by doping or in magnetic fields. In addition, examination of experimental dielectric functions reported by various authors showed that the magnitude of ε_2 is overestimated in the existing literature data for GaSb, ZnTe, ZnS, and CdSe, probably due to the neglect or incorrect treatment of possible overlayers.

DOI: 10.1103/PhysRevB.76.125203 PACS number(s): 71.20.Nr, 78.20.Ci, 78.20.Bh

I. INTRODUCTION

It is now well established that both the three highest valence bands (VBs) and the lowest conduction band (CB) of III-V and II-VI zinc-blende semiconductors are nonparabolic, nonspherical, and spin split. Details of the band structure in the vicinity of the Γ point of the Brillouin zone (BZ) are needed to correctly interpret optical and transport phenomena in three-dimensional and low-dimensional systems and remain the subject of numerous experiments and theoretical works. In early investigations of InSb, InAs, GaAs, and InP, the CB was commonly assumed to be isotropic but not parabolic. Studies of the nonparabolicity were greatly stimulated by the famous paper of Kane,[1] who derived an explicit dispersion relation for the CB in InSb. Infrared (ir) absorption and reflectance, Faraday rotation, and thermoelectric power in a high magnetic field were among the most popular experimental methods used. Experiments yielded the electron effective mass as a function of carrier density in qualitative agreement with Kane's description. It should be noted, however, that great dispersion of experimental data and, hence, considerable uncertainty regarding precise values of the electron effective mass have existed. A comprehensive review of early results for the nonparabolicity and its effects on transport phenomena in small-gap semiconductors can be found in Ref. 2. Now, it seems that the values of the electron effective mass at the bottom of the CB are well known for most of the III-V and II-VI zinc-blende semiconductors from cyclotron resonance (CR) and optically detected CR measurements.[3–7] In addition, CR investigations demonstrated the CB nonparabolicity, anisotropy and spin splitting in a number of semiconductors.[8–11] Effective masses in heavily doped n-GaAs (Ref. 12) and n-InP (Ref. 13) were obtained from Shubnikov–de Haas experiments and shown to match well the CR data at lower electron concentrations. Cardona and co-workers[14,15] used the technique of resonant Raman scattering by phonons in a magnetic field to determine the effective mass and dispersion relation in GaAs in the region from 0.1 to about 0.3 eV above the CB minimum.

For a nonparabolic CB, the nonparabolicity $E_{NP}=E_{cp}(\mathbf{k})-E_c(\mathbf{k})$ can be defined,[16] where $\mathbf{k}$ and $E_c(\mathbf{k})$ are the electron wave vector and the dispersion relation for the CB, respectively, while $E_{cp}(\mathbf{k})$ would be the electron energy assuming a parabolic band. The lowest CB of zinc-blende semiconductors is both nonparabolic and nonspherical (warped), which is related to the wave function mixing due to coupling to other valence and conduction bands.[1,16,17] In addition, owing to a lack of inversion symmetry of the crystal lattice, the lowest CB is also spin split (except for $\mathbf{k}$ parallel to the [100] and [111] directions).[16] The CB spin splitting has a maximum value for $\mathbf{k}\parallel[110]$ and varies as k^3 for sufficiently small k.[17,18] As a result, the CB nonparabolicity depends on the direction of $\mathbf{k}$ being the smallest for $\mathbf{k}\parallel[100]$ and the largest for $\mathbf{k}\parallel[111]$, as revealed by calculations.[16,17] Generally, the nonsphericity and spin splitting of the CB close to the BZ center are small compared with the nonparabolicity. For example, in GaAs, provided that the wave vector corresponds to electron states at the Fermi level in a strongly degenerate semiconductor with an electron concentration $n_e=10^{19}$ cm^{-3}, the average of E_{NP} is about 45 meV, while the difference between E_{NP} values for the two principal directions is only about 10 meV (Refs. 16 and 17) and the spin splitting is less than 5 meV.[17,18] In this paper, we will neglect the nonsphericity and spin splitting of the CB. We will assume a spherical CB and concentrate exclusively on the study of nonparabolicity effects.

Currently, experimental data for the CB nonparabolicity are primarily limited by obtainable doping levels, magnetic fields, and sample quality. For the most studied small-gap (InSb, InAs) and medium-gap (GaAs, InP) semiconductors, they are restricted to an electron energy of about 0.5 eV (Ref. 2) and 0.3 eV,[15,17] respectively. Quantitative experimental data for other III-V and II-VI binary compounds are rather scarce and will be reviewed in Sec. IV. Recently, we have shown that the CB nonparabolicity can be derived from a comparison between the experimental and calculated imaginary parts ε_2 of the dielectric function (DF).[19,20] The goal of this work is the determination of the CB dispersion relation in altogether 12 III-V and II-VI zinc-blende semiconductors. Our approach is based upon analyzing excitonic and direct band-to-band optical transitions between the three highest VBs and the lowest CB in a spectral region close to and above the fundamental absorption edge. Electron energies which can be studied in this way are expected to be significantly higher than those achievable by doping or in magnetic fields.

In our investigation, GaAs and InP serve as model materials to test the validity of the method used. We demonstrate that our results are in excellent agreement with those available in the literature. In addition, we expand the experimental data on the nonparabolicity in these semiconductors to significantly higher electron energies. For completeness, InSb and InAs were also included into the analysis, although the accessible energy range is relatively narrow in this case. As for other semiconductors, we obtained experimental data for the CB nonparabolicity and effective mass in the region from the bottom of the CB up to electron energies between 0.6 and 2.2 eV depending on the semiconductor of interest.

The paper is organized as follows. In the next section, the method we used is described. Section III addresses effects caused by the complex VB structure. We investigate how the uncertainty of Luttinger parameters influences the accuracy of the method. In Sec. IV, the determined CB nonparabolicity and effective mass as a function of the wave vector and free electron concentration are reported and compared with data available in the literature. In Sec. V, experimental results of the present study are analyzed in terms of correspondence to simple models of the CB structure based on the **kp** theory. In particular, we can conclude that the magnitude of ε_2 is overestimated in existing experimental data for some semiconductors. A summary is given in Sec. VI.

II. METHOD: FORMULATION AND GENERAL REMARKS

In the present work, we obtain data on the CB nonparabolicity by adjusting the calculated imaginary part ε_2 of the DF to the experimental one. Experimental ε_2 data were taken from the literature (see Secs. IV and V for references and discussion of the choice made). An explicit description of the model for ε_2 and calculation procedure is given in our previous paper,[20] where the intensity of excitonic absorption in III-V semiconductors was studied. We showed that, in order to achieve the quantitative agreement with experiment, the excitonic contribution to ε_2 has to be weighted in favor of the band-to-band transitions by a factor f_x that lies between zero and unity. Data points for various semiconductors and temperatures are well described by a fitting function

$$f_x = \frac{(\lambda_p/a_x)^{b_0}}{b_1 + (\lambda_p/a_x)^{b_0}}, \tag{1}$$

where λ_p and a_x are the phonon mean free path and exciton Bohr radius, respectively, $b_0=1.32$ and $b_1=0.764$. Then, the expression for calculating ε_2 is as follows:

$$\varepsilon_2(E) = f_x\varepsilon_2^{DX}(E) + \frac{A_0 m_0 E_P}{16\pi^2 E^2}\sum_v \int_{BZ} (1 + f_x S_v) F_v(\mathbf{k})\,\delta[E_c(\mathbf{k}) - E_v(\mathbf{k}) - E]\,d\mathbf{k}, \tag{2}$$

with

$$\varepsilon_2^{DX}(E) = \frac{A_0 m_0 E_P}{2E^2}\left(\frac{8\pi\varepsilon_0\varepsilon_s}{e^2}\right)^3 \sum_v \sum_{n=1}^{\infty} F_v^{DX}\left(\frac{E_b}{n}\right)^3 \times \delta\left(E - E_{gv} + \frac{E_b}{n^2}\right) \tag{3}$$

and

$$S_v = (2\pi\sqrt{\varepsilon_v})/[1 - \exp(-2\pi/\sqrt{\varepsilon_v})], \tag{4}$$

where E is the photon energy, the first and the second terms in Eq. (2) describe contributions due to discrete excitonic states and Coulomb-enhanced band-to-band transitions, respectively, $A_0=\hbar^2e^2/\varepsilon_0 m_0^2$, $\hbar$ is the Planck constant, e and m_0 are the free electron charge and mass, respectively, ε_0 is the electric constant, E_P is the momentum matrix element in energy units, v denotes the heavy-hole (HH), light-hole (LH), or split-off hole (SH) VB, S_v is the Sommerfeld factor, $F_v(\mathbf{k})$ is a dimensionless wave-vector-dependent quantity proportional to the transition probability between the VB v and the CB, $E_v(\mathbf{k})$ is the dispersion relation in the VB v, ε_s is the static dielectric constant, F_v^{DX} specifies the oscillator strength of the exciton series belonging to the VB v ($F_v^{DX}=2/3$ for an unstrained zinc-blende crystal[20]), E_b is the exciton binding energy which is assumed to be identical for all three exciton series belonging to the HH, LH, and SH VBs, E_{gv} is the energy gap between the CB and the VB v at $\mathbf{k}=0$, and $\varepsilon_v=(E-E_{gv})/E_b$. The VB structure and transition probabilities are calculated making use of Luttinger parameters γ_1, γ_2, and γ_3 and spin-orbit splitting Δ_{so} by solving the 6×6 Hamiltonian for eigenfunctions and eigenvalues. The CB dispersion relation in Eq. (2) is taken in the form

$$E_c(\mathbf{k}) = \frac{\hbar^2}{2m_0}\frac{\mathbf{k}^2}{m_{e0}^*} + \sum_{i=1}^{i_0} N_i\left(\frac{\mathbf{k}^2}{m_{e0}^*}\right)^{i+1}, \tag{5}$$

where m_{e0}^* is the electron effective mass at the CB bottom in units of the free electron mass, N_i are the nonparabolicity coefficients, and the electron energy is counted from the CB bottom. To compare a calculated $\varepsilon_2(E)$ with an experimental spectrum, the broadening has to be incorporated. We use the Gaussian line-shape function with σ as the broadening parameter. Arguments in favor of the Gaussian broadening as compared with the Lorentzian one have been given previously.[20]

For a spherical band, the nonparabolicity coefficients N_i do not depend on the direction of $\mathbf{k}$, and the CB dispersion relation expressed by Eq. (5) can equivalently be written as follows:

$$E_c = \hbar^2k^2/(2m_0 m_e^*), \tag{6}$$

where the quantity

$$m_e^* = m_{e0}^* \left(1 + \sum_{j=1}^{j_0} M_j E_c^j \right) \tag{7}$$

has a meaning of the energy-dependent (or wave-vector-dependent) effective mass, with M_j representing a new (but equivalent to N_i) set of nonparabolicity coefficients. In the description of many transport and optical phenomena, the momentum (or dynamical) effective mass m_p arises,[2] which is defined as $1/m_p = (1/\hbar^2 k)(dE_c/dk)$. From Eqs. (6) and (7), we have

$$m_p^* = m_{e0}^* \left[1 + \sum_{j=1}^{j_0} (j+1) M_j E_c^j \right], \tag{8}$$

where m_p^* is the electron momentum effective mass in units of the free electron mass. In the limiting case of a strong degeneracy of a semiconductor, there is a simple relation[2]

$$k_F^2 = (3\pi^2 n_e)^{2/3} \tag{9}$$

between the Fermi wave vector k_F and the electron concentration n_e. Introducing it in Eq. (5) yields the dependence of the Fermi level on the carrier density. Finally, combining Eqs. (5)–(9), the momentum effective mass can be obtained as a function of electron concentration, provided that the semiconductor is strongly degenerate.

Assuming only the first coefficient M_1 to be nonzero in Eq. (7), the simplest dispersion relation for a nonparabolic spherical band is obtained, which can be written as follows:

$$\hbar^2 k^2 / (2 m_0 m_{e0}^*) = E_c (1 + E_c / E^*), \tag{10}$$

where E^* is a constant. This leads to a linear dependence of the momentum effective mass on electron energy:

$$m_p^* = m_{e0}^* (1 + 2E_c / E^*). \tag{11}$$

Equation (10) and (11) are frequently used to account for nonparabolicity effects observed in various experiments.[2,12,17]

Now, we briefly address the procedures used. Values of input parameters (m_{e0}^*, E_P, E_b, ε_s, and f_x) to calculate ε_2 for III-V semiconductors are identical to those presented in Ref. 20. The only exception is GaN (see Sec. IV A for more details). Varying coefficients N_i in Eq. (5) and the broadening parameter σ to adjust the calculated ε_2 spectrum to the experimental one over a wide spectral region, we obtain the CB dispersion relation $E_c(k)$, which is then fitted by Eqs. (6) and (7) to determine the coefficients M_j. Terms up to $i_0=8$ and $j_0=4$ were included in Eqs. (5) and (7), respectively. The results are presented and discussed in Secs. IV and V.

The problem is more complicated if we consider II-VI semiconductors. First of all, the momentum matrix element E_P is known with great uncertainty for these materials, and we cannot obtain reliable data for the factor f_x by a direct comparison of the calculated ε_2 with experiment, as it was done for III-V semiconductors in Ref. 20. In addition, sets of Luttinger parameters are not established yet. Therefore, we estimate f_x using Eq. (1) and present composite Luttinger parameter sets deduced from existing literature data. Details of the procedure are given in Sec. IV B. Then, the values of E_P and the CB dispersion relation are determined from comparison of calculated and experimental ε_2 spectra.

For the sake of understanding how much details of the VB structure can affect the determined CB dispersion relation, different sets of Luttinger parameters proposed for GaAs and InP are compared in the next section.

III. EFFECTS OF THE COMPLEX VALENCE-BAND STRUCTURE

For most of III-V and II-VI zinc-blende semiconductors, numerous sets of Luttinger parameters have been obtained from various experiments and calculations. In general, use of different sets leads to somewhat differing results for the CB dispersion relation. In this situation, a composite set of Luttinger parameters can benefit. Arguments for and procedure to introduce it will be given below. To study possible effects of the VB structure, we compare sets proposed for GaAs and InP (see Table I). Note that other important input parameters are known with great precision for these semiconductors. To illustrate the differences between the sets, we calculated the effective mass of holes $m_v^*(\mathbf{k})$ defined by

$$\frac{\hbar^2 \mathbf{k}^2}{2 m_0 m_v^*(\mathbf{k})} = E_v'(\mathbf{k}), \tag{12}$$

where $E_v'(\mathbf{k})$ is the dispersion relation in the VB v and the hole energy is counted down from the top of the VB v. Effective masses given by Eq. (12) at $k=0$ for the three principal directions are the same ones which can be directly calculated using the expressions involving Luttinger parameters.[3] One can find that, for most sets, the HH VB exhibits a significant anisotropy but is only slightly nonparabolic, while the LH and SH bands are both nonparabolic and nonspherical. Table I lists the HH effective mass at $k=0$ in the [100] and [111] directions, as well as the LH effective mass in the [111] direction for $k=0$ and $k=k_0$, with $k_0 = 0.84\ \text{nm}^{-1}$, to demonstrate the anisotropy and nonparabolicity of the VB. Note that conduction-band states described by a wave vector k_0 would be those of electrons at the Fermi level in a strongly degenerate semiconductor with $n_e = 2 \times 10^{19}\ \text{cm}^{-3}$. It can be seen in Table I that discrepancies occur between different sets regarding the resulting effective masses, anisotropy, and nonparabolicity. Sometimes, this is quite significant (compare, e.g., sets proposed by Bimberg *et al.*[132] as well as by Pfeffer and Zawadzki[17(b)] for InP) meaning that the shape of the constant-energy surface over which the integration in Eq. (2) is carried out can greatly vary from set to set. Note that the transition probability described by the quantity $F_v(\mathbf{k})$ also changes.

To study the effects of details of the VB structure, we adopted the following procedure. The factor f_x that determines excitonic contributions to ε_2 was fixed at 0.67 and 0.78 (Ref. 20) and experimental ε_2 from Refs. 21 and 22 were taken for GaAs and InP, respectively. Other input parameters are quoted in Ref. 20. Composite sets of Luttinger parameters for GaAs and InP were derived by averaging the spherical parameter μ, the cubic parameter δ, and the HH effective mass m_{HH}^* along the [100] direction at $k=0$. The

TABLE I. Luttinger parameters for GaAs and InP obtained from experiments or calculations by various authors as well as the resulting effective masses of heavy holes at $k=0$ in the [100] and [111] directions and of light holes in the [111] direction for $k=0$ and $k=k_0$. For a detailed explanation of k_0, E_P, E^*, and X_s values, see Eqs. (2), (10), and (14) and related paragraphs.

Reference	γ_1	γ_2	γ_3	m^*_{HH} at $k=0$		m^*_{LH} for [111]		E_P (eV)	E^* (eV)	X_s
				[100]	[111]	$k=0$	$k=k_0$			
					GaAs					
117	7.2	2.5	2.5	0.455	0.455	0.082	0.125	28.2	1.18	1.25
118	6.77	2.28	2.88	0.452	0.990	0.080	0.140	27.2	1.35	1.31
70	7.65	2.41	3.28	0.353	0.917	0.070	0.133	28.9	1.26	1.25
119	7.10	2.32	2.54	0.407	0.495	0.082	0.127	28.4	1.22	1.26
120	6.98	2.25	2.88	0.403	0.820	0.079	0.136	27.4	1.30	1.29
121	6.85	2.10	2.90	0.377	0.952	0.079	0.139	27.4	1.33	1.29
122	7.05	2.35	3.00	0.426	0.952	0.077	0.137	27.4	1.33	1.29
123	7.06	2.22	3.01	0.382	0.962	0.077	0.137	27.6	1.33	1.29
75	7.17	2.88	2.91	0.709	0.741	0.077	0.133	27.2	1.36	1.30
124	6.790	1.924	2.681	0.340	0.700	0.082	0.135	27.8	1.27	1.28
125	6.80	1.90	2.73	0.333	0.746	0.082	0.136	27.8	1.29	1.28
76	7.20	2.15	3.05	0.345	0.909	0.075	0.136	27.8	1.33	1.27
126	7.10	2.02	2.91	0.327	0.781	0.077	0.134	28.1	1.30	1.27
17(b)	7.80	2.46	3.30	0.347	0.833	0.070	0.131	28.4	1.30	1.24
127	6.67	1.87	2.67	0.341	0.752	0.083	0.137	27.7	1.29	1.29
3	6.98	2.06	2.93	0.350	0.893	0.078	0.137	27.6	1.30	1.28
128	7.18	2.23	2.99	0.368	0.833	0.076	0.135	27.9	1.30	1.27
This work[a]	6.85	2.16	2.79	0.353	0.917	0.070	0.133	27.6	1.31	1.29
					InP					
129	5.75	1.39	2.05	0.337	0.606	0.102	0.249	22.4	1.47	1.25
70	6.28	2.08	2.76	0.472	1.32	0.085	0.312	21.1	1.61	1.27
130	5.04	1.56	1.73	0.521	0.633	0.118	0.258	21.2	1.50	1.31
131	5.15	0.94	1.62	0.306	0.524	0.119	0.239	22.1	1.38	1.27
132	4.95	1.65	2.35	0.606	4.00	0.104	0.377	19.8	1.76	1.37
133	5.22	1.83	2.34	0.641	1.85	0.101	0.340	20.2	1.72	1.34
17(b)	6.56	1.75	2.32	0.327	0.521	0.089	0.232	22.7	1.27	1.19
134	5.05	1.60	1.73	0.541	0.629	0.118	0.257	21.1	1.50	1.32
25	4.94	1.50	1.99	0.515	1.04	0.112	0.302	20.3	1.54	1.34
3	5.08	1.60	2.10	0.532	1.14	0.108	0.308	20.7	1.62	1.34
This work[a]	5.09	1.50	1.98	0.480	0.886	0.111	0.288	21.2	1.59	1.32

[a] Composite set; see Eq. (13) and text.

above quantities were calculated from the reported Luttinger parameters as follows:[23]

$$\mu = \frac{6\gamma_3 + 4\gamma_2}{5\gamma_1}, \quad \delta = \frac{\gamma_3 - \gamma_2}{\gamma_1}, \quad m^*_{HH} = \frac{1}{\gamma_1 - 2\gamma_2}. \qquad (13)$$

The resulting sets of Luttinger parameters are close to those of Vurgaftman *et al.*[3] (see Table I), who also averaged literature data but did not specify explicitly the details of the procedure. For each set of Luttinger parameters shown in Table I, the ε_2 spectrum was calculated. To adjust it to the experimental one, the momentum matrix element E_P and nonparabolicity coefficients N_i were varied.

Figure 1 shows fits (solid lines) to experimental ε_2 spectra (circles) for GaAs and InP using the composite sets of Luttinger parameters. In Fig. 2, the resulting CB dispersion relations are presented (solid lines). For comparison, calculated ε_2 spectra and dispersion relations assuming a parabolic CB are also shown by dotted lines to demonstrate that deviations from a parabolic approximation are not small and can be detected starting at low electron energies. Use of other sets of Luttinger parameters results in fitting curves which are practically indistinguishable from those in Fig. 1. However, the adjusted values of E_P and N_i differ. The E_P values are collected in Table I, while CB dispersion relations mostly deviating from that obtained using the composite sets are shown in Fig. 2 by dotted and dashed lines. These occur

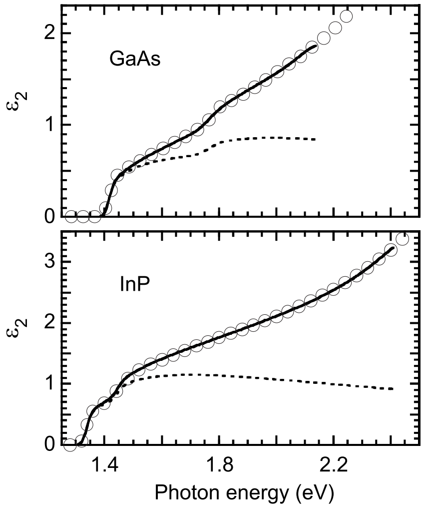

FIG. 1. Fits (solid lines) to experimental ε_2 data (circles) for GaAs and InP considering the conduction-band nonparabolicity. For comparison, calculated ε_2 spectra assuming a parabolic conduction band are shown by dotted lines.

when sets of Vrehen[117] and Neumann *et al.*[75] for GaAs, as well as sets of Bimberg *et al.*[132] and of Pfeffer and Zawadzki[17(b)] for InP, are used.

To obtain a simple quantitative measure of the nonparabolicity, we employed Eq. (10) and calculated the value E^* to match the determined dispersion relation $E_c(k)$ at a given k. The inset of Fig. 2 shows that E^* deduced in this way depends on the wave vector. Values of E^* related to $k=k_0$ are presented in Table I. As seen, E_P and E^* are not very sensitive to details of the VB structure. This can be understood as follows. For parabolic conduction and valence bands with effective masses m_e and m_h, respectively, the imaginary part ε_2 of the DF is proportional to $E_P(m_r)^{3/2}$, where $m_r = m_e m_h/(m_e+m_h)$.[24] Considering the HH and LH VBs to contribute to ε_2 close to the band gap and using the spherical approximation for the VB,[23,25] we can expect that a relation $E_P \sim 1/X_s$ should be approximately satisfied, where

$$X_s = \left(\frac{m_{hs}^*}{m_{e0}^* + m_{hs}^*}\right)^{3/2} + \left(\frac{m_{ls}^*}{m_{e0}^* + m_{ls}^*}\right)^{3/2}, \tag{14}$$

$$m_{hs}^* = 1/(\gamma_1 - 2\gamma), \quad m_{ls}^* = 1/(\gamma_1 + 2\gamma), \quad \gamma = (3\gamma_3 + 2\gamma_2)/5. \tag{15}$$

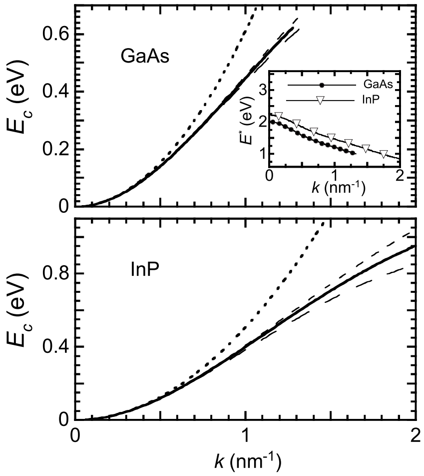

FIG. 2. Conduction-band dispersion relations determined from fits to ε_2 spectra for GaAs and InP using different Luttinger parameter sets: solid lines for composite sets (see Table I); dashed lines for sets by Vrehen[117] (GaAs) and Bimberg *et al.*[132] (InP); and long-dashed lines for sets by Neumann *et al.*[75] (GaAs) and Pfeffer and Zawadzki[17(b)] (InP). For comparison, parabolic dispersions are indicated by dotted lines. The inset shows E^* values [see Eq. (10) and text] with dependence on wave vector calculated from the conduction-band dispersion relations for GaAs and InP, which were determined using the composite Luttinger parameter sets.

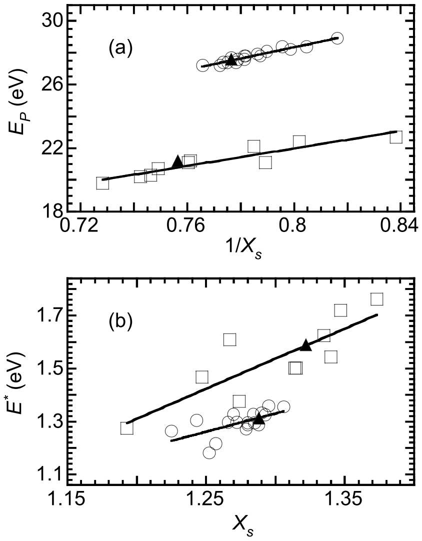

FIG. 3. (a) Momentum matrix element and (b) E^* value at $k = k_0$ in dependence on $1/X_s$ and X_s, respectively, for GaAs (circles) and InP (squares). For the meaning of X_s and k_0, see Eq. (14) and text. Data points resulting from the composite sets of Luttinger parameters are shown by filled triangles.

Values X_s calculated using $m_{e0}^*=0.0624$ and $m_{e0}^*=0.0752$ for GaAs and InP,[20] respectively, are presented in Table I. Their deviations from the average are relatively small, which explains why the determined E_P values are weakly sensitive to different sets of Luttinger parameters. In addition, as seen in Fig. 3(a), the relationship $E_P = C/X_s$ is indeed well fulfilled, with C being 35.4 and 27.5 eV for GaAs and InP, respectively. As for the quantity E^*, one can expect its dependence not only on hole masses at $k=0$ but also on the nonparabolicity and anisotropy of the VBs. However, we did not carry out a detailed analysis. As shown in Fig. 3(b), a trend of E^* to grow with increasing X_s is observed. Linear fit by $E^* = C_0 X_s - C_1$ yields $C_0 = 1.38$ eV, $C_1 = 0.466$ eV for GaAs and $C_0 = 2.27$ eV, $C_1 = 1.42$ eV for InP, respectively. Scattering of data points indicates that E^* is more sensitive to details of the VB structure than E_P.

From a practical point of view, data of Table I and Fig. 3 can be used to estimate the error of the method caused by uncertainty of Luttinger parameters. With this in mind, we introduce a quantity

$$D_{LP} = \frac{1}{X_c}\left[\frac{1}{N}\sum_{i=1}^{N}(X_{si}-X_c)^2\right]^{1/2}, \tag{16}$$

where N is the number of Luttinger parameter sets to be considered, and X_{si} and X_c correspond to a set i and the composite set, respectively, and are calculated by Eq. (14). Considering linear dependences in Fig. 3 and using Eq. (10), we have

$$\frac{\Delta E_P}{E_P} = D_{LP}, \tag{17}$$

$$\frac{\Delta E^*}{E^*} = \left(1 + \frac{C_1}{E^*}\right)D_{LP}, \quad \frac{\Delta E_c}{E_c} = \left(1 + \frac{C_1}{E^*}\right)\frac{E_c}{E^* + 2E_c}D_{LP},$$

where ΔE_P, ΔE^*, and ΔE_c are errors of values for E_P, E^*, and E_c determined. Estimates using Eqs. (17) and data in Table I as well as in Fig. 3 yield the error of E_P of about 1.9% and 4.2% for GaAs and InP, respectively, and a somewhat larger error of E^*. The error in the determination of E_c increases with increasing electron energy. At $k=k_0$, it amounts to about 0.4% and 1.0% for GaAs and InP, respectively.

Results of Secs. II and III can be summarized as follows. Differences between sets of Luttinger parameters have no dramatic effect on the determined CB dispersion relation. It allows a composite set to be used in analyzing experimental ε_2 data. The expected error in determination of the momentum matrix element and CB dispersion relation caused by uncertainty of Luttinger parameters is within several percent. In addition, it follows from Eqs. (2) and (3) that the value of E_P will be directly affected by experimental uncertainty in m_{e0}^*, E_b, and ε_s, which is also about several percent. However, the influence on the determined nonparabolicity is small, provided E_P is treated as an adjusted parameter, as revealed by tests using different values of the above input parameters in the calculations. Another important factor is the reliability of experimental data for ε_2. This question is discussed in Sec. V, where data from various sources for the DF of several semiconductors are analyzed.

IV. RESULTS AND COMPARISON WITH LITERATURE DATA

In this section, the CB dispersion relation, nonparabolicity, and effective mass are reported and compared with data from literature. Assuming a strongly degenerate semiconductor and combining Eqs. (5)–(9), the momentum electron effective mass is presented as a function of free electron concentration. Such dependence is most frequently deduced from experiments. Experimental ε_2 spectra, which we compare with calculations, have been measured at room temperature. Therefore, room-temperature values of input parameters are used in the calculations. For GaN and II-VI semiconductors, we present an explicit description regarding the derivation of composite Luttinger parameter sets and other input parameters. Since procedures for III-V and II-VI compounds are somewhat different, as briefly mentioned in Sec. II, the results are collected in two separate subsections.

A. III-V compounds

To calculate ε_2, we used our composite sets of Luttinger parameter for GaAs and InP (see Table I) and sets proposed by Vurgaftman *et al.*[3] for InSb, InAs, and GaSb. A composite set for GaN was derived considering overall nine Luttinger parameter sets from Refs. 26–34, as described in Sec. III [see Eqs. (13)]. The result is as follows: $\gamma_1=2.77$, $\gamma_2=0.796$, and $\gamma_3=1.12$. An electron effective mass of $0.15m_0$ for zinc-blende GaN obtained from electron spin resonance measurements[35] is the only experimental result at present. However, the above value seems to be underestimated, because a considerably overestimated value of E_P=28 eV (see Sec. V for a more detailed discussion) was used to calculate it from the measured g factor. The average value of bare electron effective mass derived from calculations[26–34,36–38] is about $0.165m_0$. Note that the polaron electron and hole masses have been shown to be effective in excitonic and interband optical transitions close to the band gap.[39,40] Since the polaronic correction amounts to about 10% in GaN,[39] we adopt a value of $m_{e0}^*=0.18$ for the polaron electron effective mass in GaN. For other III-V compounds studied in this work, polaronic corrections are small[10] and were neglected. Other input parameters used to calculate ε_2 spectra of III-V compounds are quoted in Ref. 20 and will not be repeated here.

The calculated ε_2's were adjusted to the experimental ones reported for GaAs,[21] InP,[22] GaN,[41] GaSb,[42] as well as InAs and InSb.[43] In these studies, ε_2 data were measured on bulk crystals[21,22,42,43] and relaxed epitaxial GaN films grown on GaAs substrates.[41] The resulting nonparabolicity coefficients N_i and M_j [see Eqs. (5) and (6)] are presented in Tables II and III, respectively. The last columns of the tables indicate limiting values of the wave vector k_{lim} and electron energy $E_{c,lim}$, respectively, up to which the nonparabolicity coefficients are valid. Figure 4 presents the determined CB dispersion relations and relative electron momentum effective masses m_p/m_{e0} with dependence on electron concentration, where $m_{e0}=m_{e0}^*m_0$ is the electron effective mass at the CB bottom. Note that our data for InSb and InAs are restricted to relatively low electron concentrations. This is caused by limitations of the numerical procedure due to rapidly rising nonparabolicity coefficients. Expansion of the dispersion relation in powers of k^2, as in Eq. (5), appears to be computationally ineffective in describing electronic states far from the zone center in narrow-gap semiconductors. However, as seen in Fig. 4(a), for compounds with a larger electron effective mass, accessible energies are well above those obtainable by conventional doping.

Surprisingly little detailed quantitative data for the CB dispersion relation in III-V semiconductors close to the Γ point have been published. Only GaAs is an exception. Comparison of our results with existing literature data for GaAs (Refs. 15–17) is presented in Fig. 5(a). Since somewhat differing values of the electron effective mass at the CB bottom

TABLE II. Nonparabolicity coefficients N_i [see Eq. (5)] for the conduction band of III-V semiconductors derived from fits to ε_2 spectra. The units are $10^{10(i+1)}$ eV/m. k_{lim} denotes electron wave vectors up to which the nonparabolicity coefficients are valid.

	N_1	N_2	N_3	N_4	N_5	N_6	N_7	N_8	k_{lim} (nm^{-1})
InSb	−23.0	87.0	−115	340	−3150	7300	−21500	65000	0.45
InAs	−13.8	25.0	−25.0	840	−5100	9200	−4300	7500	0.75
InP	−7.50	12.1	−12.0	2.90	2.00	0.95	0.95	−0.05	2.0
GaSb	−12.8	32.5	−41.0	17.0	−11.5	29.5	−17.5	10.5	1.1
GaAs	−7.95	4.90	40.0	−75.0	500	−3700	4150	7700	1.4
GaN	−2.53	0.85	−0.10	0.048	−0.01	0.005	−0.006	0	4.5

were used, we compare deviations from a parabolic CB, i.e., the nonparabolicity E_{NP} (see Sec. I). Rössler[16] calculated the CB dispersion relation using a five-band 14×14 **kp** model. Squares on Fig. 5(a) are the average of the deduced nonparabolicity in the [100] and [111] directions. The circles have the same meaning and show data reported by Pfeffer and Zawadzki,[17] who calculated the band structure using a five-level **kp** model and including far-level contributions as well as polaron effects. Ruf and Cardona[15] studied resonant Raman scattering by phonons in a magnetic field. Their result is shown by the dotted line on Fig. 5(a). It is seen that our data (the solid line) are in good agreement with those of Refs. 15 and 16. In addition, we were able to measure the CB dispersion relation up to considerably higher electron energies of about 0.65 eV [see also Fig. 4(a)]. Calculations by Pfeffer and Zawadzki[17] seem to slightly overestimate the CB nonparabolicity in GaAs. In case of InP, no detailed quantitative data for the CB nonparabolicity near the Γ point have been reported. We obtained the CB dispersion relation for InP up to electron energies of about 1 eV [see Fig. 4(a)]. The resultant CB nonparabolicity of InP is shown in Fig. 6(a) by the solid line.

As reviewed in Sec. I, numerous experiments have been carried out to study the electron effective mass as a function of carrier density. Among them, low-temperature CR and optically detected CR measurements of high-quality GaAs and InP samples with low electron concentration, as well as Shubnikov–de Haas experiments at medium doping, yielded the most reliable data. In Figs. 5(b) and 6(b), these are shown by open symbols. For GaAs, also included are data of Ref. 14 derived from measurements of resonant Raman scattering by phonons in a magnetic field at 10 K. The solid lines in Figs. 5(b) and 6(b) represent our results calculated by Eqs. (5)–(9) with nonparabolicity coefficients from Tables II and III. For the sake of comparison, we have scaled our data using low-temperature values of the electron effective mass at the CB bottom of $m_{e0}^*=0.0665$ and $m_{e0}^*=0.0803$ for GaAs and InP, respectively, instead of the room-temperature ones given in Sec. II after Eq. (15). The above low-temperature effective masses practically coincide with those recommended by Vurgaftman *et al.*[3] It can be seen in Figs. 5(b) and 6(b) that our results are in excellent agreement with all low-temperature data from the literature. However, CR and Shubnikov–de Haas experiments are limited to medium electron concentrations by the requirement of high mobility of free charge carriers.[44] Extremely high carrier densities were studied by ir reflectance and thermoelectric power in a high magnetic field. Usually, such measurements are carried out at room temperature. Note that the effective masses deduced from optical and transport experiments are mean values averaged over the participating electrons. If the degeneracy is not complete, the mean values derived from different measurements can be quite different (see, e.g., Ref. 2 for a more detailed discussion). Therefore, only room-temperature data for $n_e > 2\times10^{18}$ cm^{-3} available in the literature are shown in Figs. 5(b) and 6(b) (filled symbols). These are more scattered as compared to the low-temperature ones for lower electron concentrations, which can, at least partially, be related to an overall deterioration of crystal quality at higher doping levels as well as to a possible inaccurate determination of the electron concentration. In addition, it is not clear whether effects of impurities on the band structure can be neglected at ex-

TABLE III. Nonparabolicity coefficients M_j [see Eq. (6)] for the conduction band of III-V semiconductors derived from fits to ε_2 spectra. The units are $(\mathrm{eV})^{-j}$. $E_{c,lim}$ denotes electron energies up to which the nonparabolicity coefficients are valid.

	M_1	M_2	M_3	M_4	$E_{c,lim}$ (eV)
InSb	1.65	0.811	34.9	−58.0	0.32
InAs	0.928	1.33	5.01	−6.52	0.48
InP	0.451	0.883	−1.23	1.16	0.98
GaSb	0.837	1.25	1.30	−1.38	0.67
GaAs	0.496	1.14	−1.67	1.69	0.63
GaN	0.187	0.00584	0.0417	0.00313	2.2

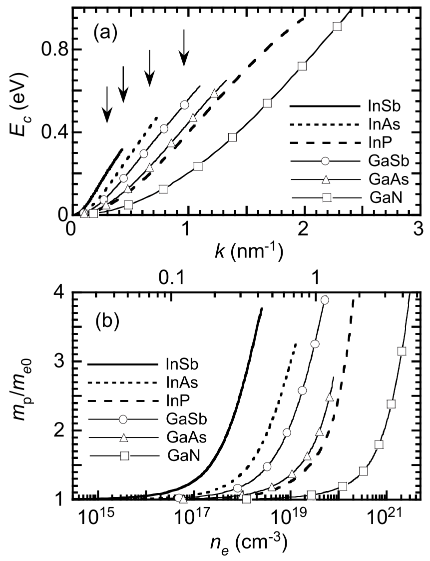

FIG. 4. (a) Conduction-band dispersion relation and (b) relative electron momentum effective mass with dependence on electron concentration for III-V semiconductors determined from fits to experimental ε_2 spectra. The arrows indicate the Fermi level position in the limiting case of a strong degeneracy for electron concentrations of 10^{18}, 3×10^{18}, 10^{19}, and 3×10^{19} cm^{-3} from left to right, respectively. In (b), the upper x axis relates the wave vector from (a) with the free electron concentration from (b).

tremely high doping. Note that in our method, experimental data obtained from measurements of high-quality samples with low defect concentrations are analyzed. A similar way has been used in Refs. 14 and 15 as well.

As for InSb and InAs, in a range of electron concentrations up to about 3×10^{18} and 1×10^{19} cm^{-3}, respectively, which is accessible to the method used in this work, our results for the effective mass [see Fig. 4(b)] are in good agreement with data available in the literature for both materials (see, e.g., Refs. 2 and 6 and references therein). In GaSb, owing to the small energy separation between the Γ and L minima (about 0.08 and 0.03 eV at low and room temperatures, respectively) and the much larger density of states at the L minimum,[45,46] a significant fraction of the electrons occupy L-valley states, and electron energies achievable by doping are not high. It was demonstrated that, in very high magnetic fields, CR signals arising from the Γ and L valleys can be observed separately.[47] Both valleys were shown to be nonparabolic in that work. Ghezzi *et al.*[48] interpreted absorption spectra close to the band gap of GaSb in terms of the nonparabolicity of the CB and the LH VB. However, to our knowledge, neither the CB dispersion relation nor the effective mass with dependence on electron concentration has been reported up to now for GaSb. Such data for cubic GaN are also absent.

B. II-VI compounds

Input parameters we used in calculating ε_2 spectra of II-VI compounds are given in Tables IV and V. Below, some remarks are provided in the explanation of the content of the tables. We need room-temperature values, while the electron effective mass and exciton binding energy are much accurately derived from low-temperature experiments. The procedure of estimating room-temperature values of m^*_{e0} and E_b from those at low temperatures is described in Ref. 20. It uses Eq. (2.15) of Ref. 3 and temperature dependence of the effective Rydberg energy. Besides which, both low- and room-temperature values of ε_s are required.

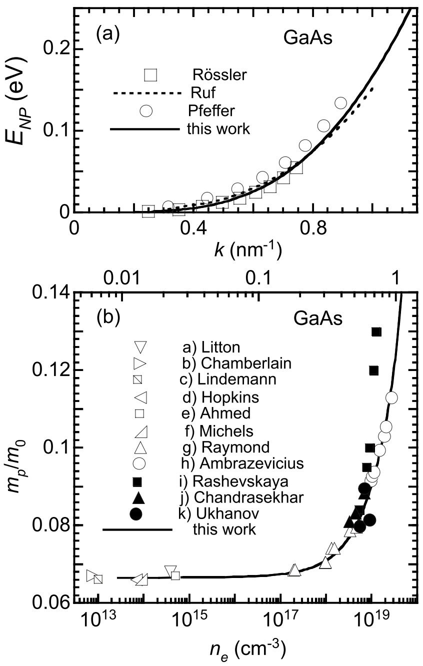

FIG. 5. (top) Nonparabolicity of the conduction band in GaAs as a function of wave vector. Squares and circles indicate averaged values for the [100] and [111] directions calculated in Refs. 16 and 17, respectively. Results of Ref. 15 (resonant Raman scattering in a magnetic field) and of this work are shown by dotted and solid lines, respectively. (bottom) Electron momentum effective mass of GaAs as a function of electron concentration. The upper x axis relates the free electron concentration with the wave vector. Data have been obtained by cyclotron resonance and optically detected cyclotron resonance measurements (Refs. 135–139 and 10), Shubnikov–de Haas experiments (Ref. 12), resonant Raman scattering in a magnetic field (Ref. 14), and ir reflectance (Refs. 140–142). Low-temperature and room-temperature data are shown by open and filled symbols, respectively. The result of this work (solid line) is calculated using nonparabolicity coefficients of Tables II and III and Eqs. (5)–(9) with a low-temperature value of the electron effective mass at the conduction-band bottom of m^*_{e0}=0.0665. (a) Ref. 135; (b) Ref. 136; (c) Ref. 137; (d) Ref. 10; (e) Ref. 138; (f) Ref. 139; (g) Ref.12; (h) Ref. 14; (i) Ref. 140; (j) Ref. 141; (k) 142; —, this work.

Low-temperature values of m^*_{e0} quoted in Table IV were obtained by averaging literature data[4,5,7] from CR and optically detected CR measurements. Note that the CR masses contain the polaronic contribution, which is not negligible in II-VI semiconductors. Low-temperature E_b values given in Table IV are also an average of literature data. In addition to the compilation of Ref. 7, recent data for ZnTe and ZnSe,[49,50] ZnS,[51,52] as well as CdTe (Ref. 53) were taken into account.

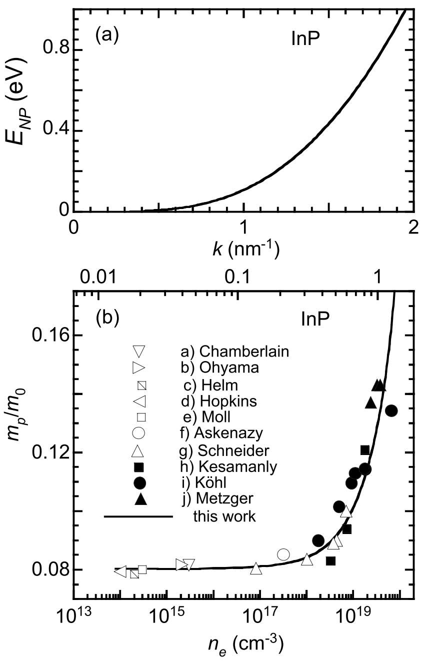

FIG. 6. (a) Nonparabolicity of the conduction band in InP as a function of wave vector determined in this work. (b) Electron momentum effective mass of InP with dependence on electron concentration. The upper x axis relates the free electron concentration with the wave vector. Data have been obtained by cyclotron resonance and optically detected cyclotron resonance measurements (Refs. 10, 135, and 143–145), Shubnikov–de Haas experiments (Ref. 13 and 146), thermoelectric power measurements (Ref. 147), and ir reflectance (Refs. 148 and 149). Low-temperature and room-temperature data are shown by open and filled symbols, respectively. The result of this work (solid line) is calculated using nonparabolicity coefficients of Tables II and III and Eqs. (5)–(9) with a low-temperature value of the electron effective mass at the conduction-band bottom of $m^*_{e0}=0.0803$. (a) Ref. 136; (b) Ref. 143; (c) Ref. 144; (d) Ref. 10; (e) Ref. 145; (f) Ref. 146; (g) Ref. 13; (h) Ref. 147; (i) Ref. 148; (j) Ref. 149;—, this work.

TABLE V. Composite sets of Luttinger parameters for II-VI semiconductors. For the meaning of related quantities N and D_{LP}, see Eq. (16).

	γ_1	γ_2	γ_3	N	D_{LP} (%)
ZnTe	3.81	0.838	1.34	11	3.0
ZnSe	3.35	0.767	1.24	11	9.2
ZnS	2.53	0.681	1.05	2	1.8
CdTe	4.64	1.46	1.92	7	3.7
CdSe	1.91	0.560	0.560	5	3.7
CdS	1.44	0.510	0.510	6	8.7

Experimental data for cubic CdSe and CdS are few and incomplete. Parameters of these two compounds given in Table IV were compiled using the results derived from studies of their wurtzite modifications.

Practically, there is no way to measure independently the static dielectric constant ε_s suitable for analyzing interband optical and magneto-optical experiments. Capacitance measurements at low frequencies usually overestimate ε_s value. On the other hand, the high-frequency dielectric constant ε_∞ and frequencies ω_{LO} and ω_{TO} of the LO and TO phonons, respectively, can be measured with high precision. Therefore, we used the Lyddane-Sachs-Teller relation[54] $\varepsilon_s/\varepsilon_\infty=(\omega_{LO}/\omega_{TO})^2$ to deduce ε_s. The high-frequency dielectric constant is the strict electronic contribution to ε_s, i.e., the dielectric constant in the absence of lattice vibrations. Most reliable data for ε_∞ are obtained if the frequency-dependent refractive index, measured well above the LO frequency but below the optical absorption edge, is extrapolated to zero frequency. In Table IV, room-temperature values of ε_∞ from prism method are presented for ZnTe, ZnSe, and CdTe,[55] as well as ZnS.[56,57] To obtain ε_∞ for CdSe and CdS, we averaged the data derived from ir reflectance measurements of wurtzite crystals,[58–60] with ε_∞ for cubic compounds being calculated by $\varepsilon_\infty=\sqrt{\varepsilon_{\infty\perp}\varepsilon_{\infty\parallel}}$, where $\varepsilon_{\infty\perp}$ and $\varepsilon_{\infty\parallel}$ are the ordinary and extraordinary high-frequency dielectric constants, respectively, observed in the wurtzite modification. This averaging procedure can be justified by noting that the value $\varepsilon_s=\sqrt{\varepsilon_{s\perp}\varepsilon_{s\parallel}}$ determines the exciton binding energy in wurtzite semiconductors (see, e.g., Ref. 39 and references therein). Phonon frequencies were taken from Refs. 7 and 61. Then, the static dielectric constant at room temperature was calculated using the Lyddane-Sachs-Teller relation. Low-temperature ε_s values were obtained using temperature dependencies reported in Refs. 62–66. Low- and room-temperature values of ε_s deduced in this way are given in Table IV. Note the very good agreement with recent results obtained from the terahertz absorption and refractive index measurements[62,67,68] for ZnTe, CdTe, and ZnS.

TABLE IV. Input parameters used for calculating ε_2 spectra of II-VI semiconductors.

	$T=0$ K			$T=300$ K					
	m^*_{e0}	E_b (meV)	ε_s	m^*_{e0}	E_b (meV)	ε_∞	ε_s	λ_p (nm)	f_x
ZnTe	0.124	13.2	9.43	0.120	12.0	7.28	9.78	10.1	0.72
ZnSe	0.145	20.1	8.38	0.141	18.1	5.90	8.73	7.3	0.71
ZnS	0.217	37.5	7.53	0.212	30.7	5.10	8.26	7.5	0.83
CdTe	0.0960	10.6	9.73	0.0915	9.2	7.21	10.3	5.7	0.47
CdSe	0.121	15.4	9.14	0.114	13.4	6.17	9.60	5.0	0.53
CdS	0.173	29.1	8.42	0.166	25.7	5.42	8.82	6.7	0.78

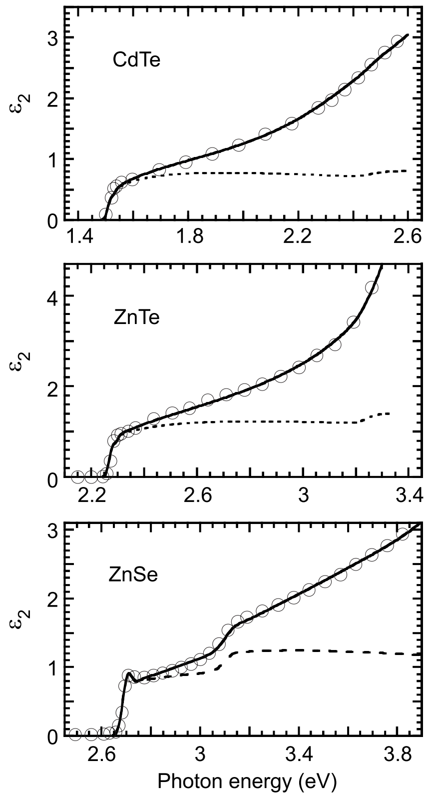

FIG. 7. Fits (solid lines) to experimental ε_2 data (circles) for CdTe, ZnTe, and ZnSe. Dotted lines show calculated ε_2 spectra assuming a parabolic conduction band.

In the two last columns of Table IV, the phonon mean free path λ_p and the factor f_x [see Eq. (1)] are presented. The former quantity was derived as described in Ref. 20. All necessary experimental data were taken from Ref. 7. The exciton Bohr radius was calculated by $a_x = e^2/(8\pi\varepsilon_0\varepsilon_s E_b)$.

Table V shows composite sets of Luttinger parameters obtained as described in Sec. III using data reported for ZnTe,[49,50,69–77] ZnSe,[49,50,70,78–85] ZnS,[70,28] CdTe,[70,75,76,53,86–88] CdSe,[25,89–92] and CdS.[91–96] Note that the VB structure parameters for CdSe and CdS are mostly known in the spherical approximation from investigations of the energy spectrum of quantum dots, which are usually assumed to be in the zinc-blende crystal structure.[25] Hence, for these two compounds, we considered only those Luttinger parameter sets, and the resulting composite sets are also in the spherical approximation, i.e., $\gamma_2 = \gamma_3$. For the meaning of related parameters, see Eq. (16).

Calculated ε_2 spectra were adjusted to experimental ones taken from Refs. 97–102 for the six studied semiconductors, respectively. The samples used in these studies were epitaxial ZnTe,[97] ZnSe,[98] and CdSe (Ref. 101) films grown on GaAs substrates, epitaxial CdTe films grown on Si,[100] epitaxial CdS films grown on InP,[102] as well as ZnS single crystals grown by a vapor-phase method.[99] There were many other measurements of the DF for II-VI compounds. More detailed discussion of the choice made is given in Sec. V. Figure 7 presents fits (solid lines) to experimental ε_2 data (circles) for CdTe, ZnTe, and ZnSe. For comparison, calculated ε_2's assuming a parabolic CB are shown by dotted lines. A remark should be made concerning ZnSe. The fit shown in Fig. 7 results in the exciton binding energy $E_b = 22.3$ meV, which is higher than that derived from literature data (see Table IV). When fitting ε_2 data reported by Kvietkova *et al.*,[103] even slightly larger E_b (22.8 meV) as well as a lower band gap energy by about 15 meV are needed. A possible explanation might be that the measured epitaxial films were strained, which can give rise to increased exciton binding energy and oscillator strength. Note that use of a lower E_b value quoted in Table IV does not significantly alter the determined CB dispersion relation, while the magnitude of the excitonic peak in the calculated ε_2 spectrum becomes underestimated.

The nonparabolicity coefficients and limits of their validity obtained from fits to experimental ε_2 spectra of II-VI semiconductors are presented in Tables VI and VII. Figure 8 is an overview of the determined CB dispersion relations and relative electron momentum effective masses with dependence on electron concentration. Many CR and optically detected CR experiments indicated a significant CB nonparabolicity in ZnTe, ZnSe, and CdTe.[4,5,11,104,105] Reported quantitative data, however, are few. In Figs. 9–12, our results (solid lines) for the CB nonparabolicity and momentum effective mass as a function of the wave vector and free electron concentration for ZnTe, ZnSe, ZnS, and CdTe are presented and compared with existing literature data (symbols) derived from CR and optically detected CR studies, magneto-optical experiments, as well as ir reflectance and Faraday rotation measurements. It can be seen from Fig. 9(a) that the determined CB nonparabolicity for ZnTe is in good agreement with calculations by Mayer and Rössler.[106] Since high-purity ZnTe and CdTe usually are of p type, light illumination was used to create the nonequilibrium carriers during CR, optically detected CR, and magneto-optical mea-

TABLE VI. The same as in Table II but for II-VI semiconductors.

	N_1	N_2	N_3	N_4	N_5	N_6	N_7	N_8	k_{lim} (nm^{-1})
ZnTe	−7.2	7.3	−3.5	2.5	−6.5	5.8	−15.5	16.8	2.1
ZnSe	−7.05	9.8	−6.5	2.3	−5.5	2.1	1.8	2.5	2.7
ZnS	−3.5	1.8	−4.0	6.2	−1.8	1.5	−1.5	1.0	3.6
CdTe	−6.8	5.5	−1.5	7.8	−16.5	13.5	−11.2	7.0	2.4
CdSe	−3.8	2.6	−1.6	0.80	−0.10	0.30	−0.49	0.164	3.6
CdS	−3.1	1.30	−0.40	0.45	−0.10	0.20	0.15	−0.55	3.8

TABLE VII. The same as in Table III but for II-VI semiconductors.

	M_1	M_2	M_3	M_4	$E_{c,lim}$ (eV)
ZnTe	0.434	1.09	−2.21	3.03	0.71
ZnSe	0.450	0.543	−0.293	0.290	1.0
ZnS	0.250	0.0396	0.0799	0.0703	1.2
CdTe	0.552	−0.267	1.30	0.187	0.93
CdSe	0.254	0.151	−0.0967	0.107	1.7
CdS	0.219	0.0408	0.0542	0.00876	1.7

surements. Hence, the determined electron effective mass is restricted to relatively low free electron concentrations [see Figs. 9(b) and 12(b)]. The electron effective mass of ZnSe and ZnS, which are usually of n type, has been measured in a larger range of electron concentrations [see Figs. 10(b) and 11(b)]. However, as is seen, in all cases, our data are extended to significantly higher electron energies than those achievable by doping. There were no reports on investigation of effects of doping in cubic CdSe and CdS, and our results for the CB nonparabolicity and wave-vector-dependent (or electron-concentration-dependent) effective mass [which can be calculated using Eqs. (5)–(9) and nonparabolicity coefficients of Tables VI and VII, see also Fig. 8] are the only ones.

V. COMPARISON TO kp MODELS AND DISCUSSION

The **kp** perturbation theory connects the dispersion relation in the vicinity of extremum points of energy bands to energy gaps and momentum matrix elements at these points.[1,109] Based on eight-band **kp** theory, a simple model of the conduction-band structure close to the Γ point in zinc-blende semiconductors can be developed, with C^* parameter accounting for effects of higher conduction bands and remote bands.[15,109] In this model, the CB dispersion relation reduces to

$$E_c(k) = \frac{\hbar^2 k^2}{2m_0}(1 + C^*) - \frac{E_g}{2} + \frac{E_g}{2}\left[1 + \frac{4E_P^*}{3E_g}\left(\frac{2}{E_g} + \frac{1}{E_g + \Delta_{so}}\right)\frac{\hbar^2 k^2}{2m_0}\right]^{1/2}, \tag{18}$$

where E_g is the energy gap between the CB and the HH valence band at $k=0$ and the momentum matrix element is denoted by E_P^* to distinguish it from that derived from ex-

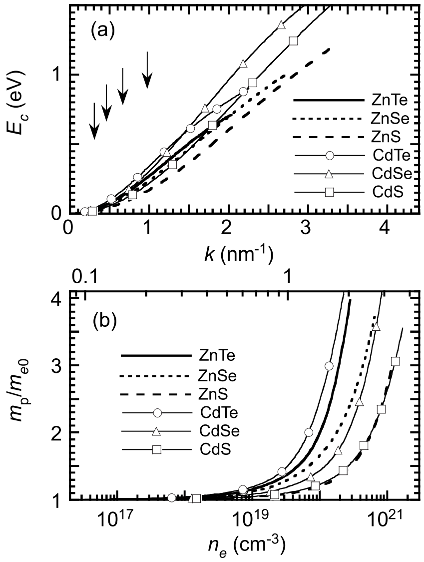

FIG. 8. The same as in Fig. 4 but for II-VI semiconductors.

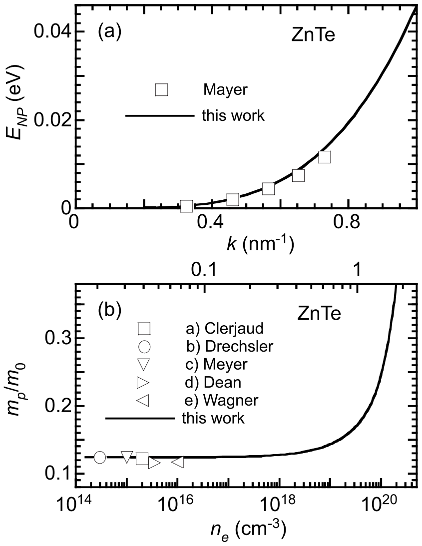

FIG. 9. (top) Nonparabolicity of the conduction band in ZnTe. Squares denote averaged values for the [100] and [111] directions calculated in Ref. 106. The result of this work is shown by the solid line. (bottom) Electron momentum effective mass of ZnTe with dependence on electron concentration. The upper x axis relates the free electron concentration with the wave vector. Data have been obtained by cyclotron resonance and optically detected cyclotron resonance (Refs. 4, 11, and 150) as well as magnetoluminescence (Refs. 77 and 151) measurements at low temperatures. The result of this work (solid line) is calculated using nonparabolicity coefficients of Tables VI and VII and Eqs. (5)–(9) with a low-temperature value of the electron effective mass at the conduction-band bottom of $m_{e0}^*=0.124$. (a) Ref. 150; (b) Ref. 11; (c) Ref. 4; (d) Ref. 151; (e) Ref. 77;—, this work.

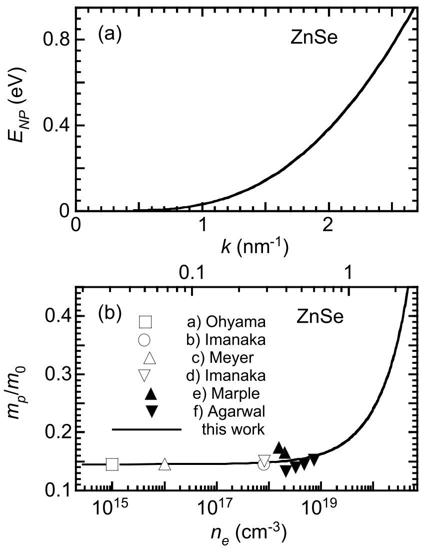

FIG. 10. (top) Nonparabolicity of the conduction band in ZnSe determined in this work. (bottom) Electron momentum effective mass of ZnSe with dependence on electron concentration. The upper x axis relates the free electron concentration with the wave vector. Data have been obtained by cyclotron resonance and optically detected cyclotron resonance (Refs. 4, 5, 104, and 105) measurements at low temperatures, as well as by Faraday rotation and ir reflectance at room temperature (Refs. 107 and 108). The result of this work (solid line) is calculated using nonparabolicity coefficients of Tables VI and VII and Eqs. (5)–(9) with a low-temperature value of the electron effective mass at the conduction-band bottom of $m_{e0}^{*}=0.145$. (a) Ref. 104; (b) Ref. 105; (c) Ref. 4; (d) Ref. 5; (e) Ref. 107; (f) Ref. 108; —, this work.

perimental ε_2 data. The electron effective mass at the bottom of the CB is given by

$$\frac{1}{m_{e0}^{*}} = 1 + C^{*} + \frac{E_P^{*}}{3}\left(\frac{2}{E_g} + \frac{1}{E_g + \Delta_{so}}\right). \tag{19}$$

It was observed by Ruf and Cardona[15] that a similar model is in excellent agreement with CB dispersions for GaAs obtained from a 16×16 Hamiltonian and from a local empirical pseudopotential calculation for energies up to 0.6 eV above the CB bottom.

Considering the electron effective mass at the bottom of the CB and the energy gaps to be known, we have only one adjusted parameter, E_P^{*}, for instance, to fit the determined CB dispersion relation by Eq. (18). The resultant E_P^{*} values are presented in Table VIII. Spin-orbit splitting energies Δ_{so} taken from Refs. 3, 6, and 7 as well as E_g, σ, and E_P values derived from fits to experimental ε_2 spectra are also collected in the same table. In Fig. 13, we compare the determined $E_c(k)$ for several semiconductors (solid lines), which can be calculated using Eq. (5) and nonparabolicity coefficients of Table VI, to that calculated by Eq. (18) employing E_P^{*} values from Table VIII (dotted lines). For more clarity, curves for different semiconductors are vertically shifted. As can be seen in Fig. 13, Eq. (18) provides a good description of experimental data for GaAs and ZnSe. Note, however, that a systematic deviation from experimental data is observed, which becomes more pronounced when a larger wave-vector range is considered, as seen in Fig. 13 for GaN and CdSe. In general, one might not expect that Eq. (18) should be equivalently valid for all semiconductors, because effects of higher

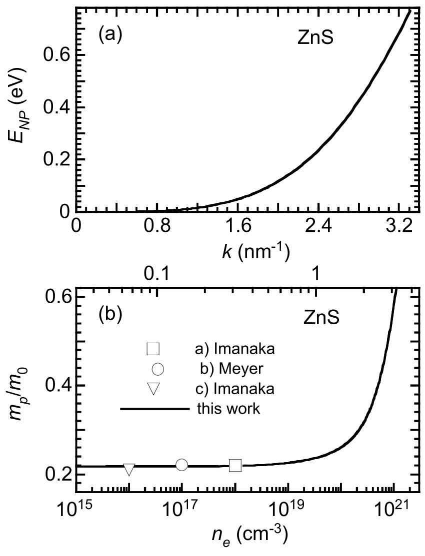

FIG. 11. The same as in Fig. 10 but for ZnS. Data shown by symbols in (bottom) of the figure have been obtained by cyclotron resonance and optically detected cyclotron resonance measurements at low temperatures. The result of this work (solid line) is calculated using $m_{e0}^{*}=0.217$. (a) Ref. 152; (b) Ref. 4; (c) Ref. 5; (d) this work.

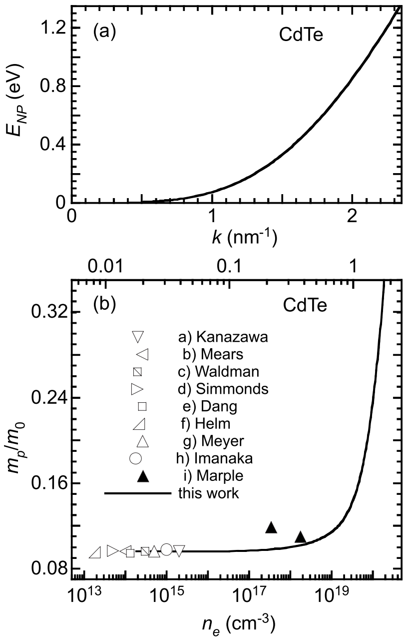

FIG. 12. The same as Fig. 10 but for CdTe. Data shown by symbols in (bottom) of the figure have been obtained by cyclotron resonance and optically detected cyclotron resonance (Refs. 4, 5, 87, 144, and 153–156) measurements at low temperatures, as well as by Faraday rotation at room temperature (Ref. 157). The result of this work (solid line) is deduced by using $m_{e0}^{*}=0.096$. (a) Ref. 153; (b) Ref. 154; (c) Ref. 155; (d) Ref. 156; (e) Ref. 87; (f) Ref. 144; (g) Ref.4; (h) Ref. 5; (i) Ref. 157; —, this work.

TABLE VIII. Spin-orbit splitting energies Δ_{so} taken from Refs. 3, 6, and 7 as well as values of E_g, σ, and E_P derived from fits to experimental ε_2 data referred to in the second column of this table. E_P^* values are from fit of the determined conduction-band dispersion relations by Eq. (18), while E^* ones are obtained in a way that Eq. (10) matches the determined conduction-band dispersion relations at $k=k_0$.

	Reference for ε_2	Δ_{so} (eV)	E_g (eV)	σ (meV)	E_P (eV)	E_P^* (eV)	E^* (eV)
InSb	43	0.81	0.171	9.0	23.3	21.8	0.16[a]
InAs	43	0.39	0.354	8.2	21.5	19.0	0.36[a]
InP	22	0.108	1.344	8.0	21.2	19.6	1.59
GaSb	42	0.76	0.710	18	34.5	25.8	0.65
GaAs	21	0.341	1.418	8.9	27.6	26.3	1.31
GaN	41	0.017	3.241	25.0	18.7	18.5	5.53
ZnTe	97	0.97	2.290	8.0	37.3	28.0	1.72
ZnSe	98	0.42	2.725	13.0	25.3	26.7	1.85
ZnS	99	0.068	3.725	50	28.5	21.0	3.97
CdTe	100	0.95	1.524	7.0	20.0	22.2	1.73
CdSe	101	0.42	1.680	8.0	23.8	15.8	3.53
CdS	102	0.067	2.465	30	18.4	14.9	4.46

[a] Extrapolated from lower electron concentrations.

bands are taken into account only up to k^2 terms. For example, Pfeffer and Zawadzki[17] argued in favor of explicit accounting for higher conduction levels Γ_8^c and Γ_7^c within a five-level **kp** model for GaAs and InP. Note also that the experimentally observed behavior of $E_c(k)$, i.e., a superlinear dependence on k at small k and a sublinear one at larger k, qualitatively agrees with *ab initio* band structure calculations (see, e.g., Refs. 15, 25, 27, 32, 33, 36, and 101). However, as is well known,[18] despite a qualitatively correct band structure over a whole Brillouin zone, important band parameters derived from *ab initio* calculations, such as the band gap and electron effective mass, have an insufficient degree of accuracy (e.g., m_{e0}^* can deviate from experiment as much as 10%–30%). In view of this, a direct comparison of *ab initio* results to the CB dispersion relation determined in the present work in a relatively narrow region near the Γ point seems to be not reasonable. A more detailed discussion is out of the scope of this paper and can be found elsewhere.[18,25] As for values E_P^* and E_P (see Table VIII), they coincide for most semiconductors within experimental accuracy, which is about several percent. However, for GaSb, ZnTe, ZnS, and CdSe, the discrepancy is obviously too large. This is illustrated in Fig. 13(b) for ZnTe and CdSe by dashed lines calculated using Eq. (18) with E_P^* taken to be equal to E_P. Such a large discrepancy implies that E_P values of 37.3 and 23.8 eV for ZnTe and CdSe derived from fits to ε_2 data of Refs. 97 and 101, respectively, are too high, indicating an overestimated magnitude of the experimental ε_2. The same conclusion is also valid to ε_2 sets for GaSb (Ref. 42) and ZnS.[99]

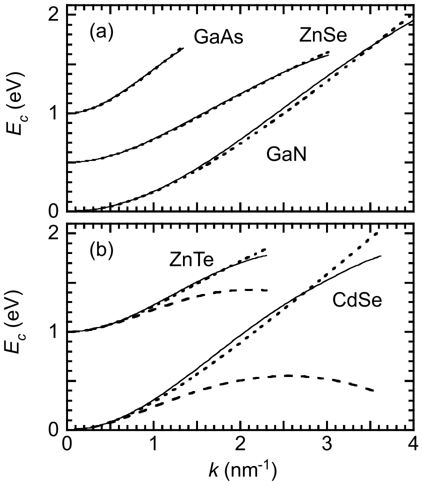

FIG. 13. Comparison of the determined conduction-band dispersion relation for several semiconductors (solid lines) to calculation by Eq. (18) with E_P^* values from Table VIII (dotted lines). Dashed lines show the calculated result for ZnTe and CdSe when E_P^* is taken to be equal to E_P (see Table VIII). For more clarity, curves for ZnSe as well as those for GaAs and ZnTe are vertically shifted by 0.5 and 1 eV, respectively.

In order to confirm this assumption, we have examined ε_2 data reported by various authors. All of them were obtained by reflectance spectroscopic ellipsometry (SE), sometimes in combination with other experimental techniques. In measuring the intrinsic bulk DF above the absorption edge, a general problem of SE is that the result is highly sensitive to a possible overlayer caused by roughness, native oxides, and contaminations of the sample surface. Effects of an overlayer can be minimized by proper chemical surface treatments and/or mathematically correcting ε_2 data by calculations within the bulk-overlayer-ambient model. It seems, however, that no perfect way exists to do it, and, usually, there are discrepancies between ε_2 data from different sources. Examples to follow illustrate effects of overlayers. Data of Ref. 41 for cubic GaN shown by circles in Fig. 14(a) were obtained from SE and reflectance investigations of many samples by multiple-sample fit considering the presence of a

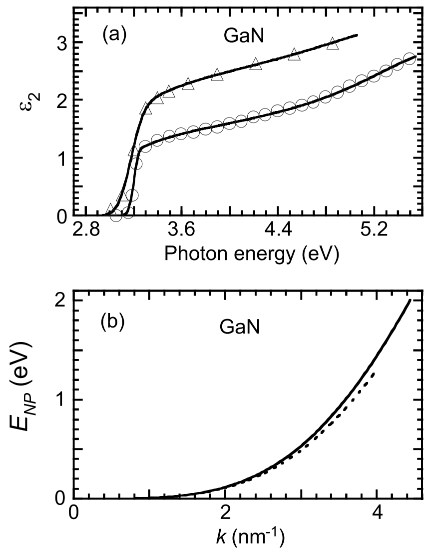

FIG. 14. (a) Fits (solid lines) to experimental ε_2 data for GaN from Ref. 41 (circles) and Ref. 110 (triangles). The resultant conduction-band nonparabolicity is shown in part (b) of the figure by solid and dotted lines, respectively.

thin surface layer. On the contrary, Muñoz *et al.* (triangles)[110] analyzed SE spectra of their sample assuming sharp boundary to ambient. Fits to both data sets [solid lines in Fig. 14(a)] yield noticeably differing E_P values (18.7 and 29.7 eV, respectively) but very close results for the CB nonparabolicity, as seen in Fig. 14(b). Note also that the broadening and the band gap energy should be treated as adjusted parameters to obtain good fits. Data for GaSb are shown in Fig. 15. SE studies by Muñoz *et al.*[42] and Ferrini *et al.*[111] yielded nearly identical ε_2 spectra shown in Fig. 15(a) by circles and triangles, respectively. Somewhat different data were deduced from transmission measurements close to the band gap by Ghezzi *et al.*[112] [squares in Fig. 15(a)]. Satisfactory fits [solid lines, Fig. 15(a)] to the data sets can be obtained using the same nonparabolicity coefficients [which are presented in Table VI and result in the CB nonparabolicity shown in Fig. 15(b)] but different E_P (34.5 and 27.9 eV, respectively). The latter E_P value is close to E_P^* obtained from fit of the determined CB dispersion relation by Eq. (18) (see Table VIII), indicating that transmission measurements could be very helpful in deducing a correct magnitude of ε_2. However, such measurements require very thin samples and can be performed only in a narrow spectral region close to the band gap where the absorption coefficient is not too high. Fitting ε_2 data for II-VI semiconductors reported by various authors, we obtained the following values of E_P: 43 eV for ZnTe;[113] 25.0 eV,[103] 31.3 eV,[114] and 40 eV (Ref. 115) for ZnSe; and 35 eV for CdTe.[116] All of them, except for Ref. 103, are higher than those presented in Table VIII. However, similar to GaN and GaSb, variations in nonparabolicity coefficients were found to be much less important than those in E_P. Calculations also show that especially the magnitude of ε_2 is affected by a thin overlayer. Its influence on the spectral course of ε_2 is of less importance considering a relatively narrow spectral range studied in this work. Thus, the determined CB nonparabolicity is expected to be roughly independent of the presence of an overlayer, while the magnitude of ε_2 will be absorbed by E_P, as it can be seen from Eqs. (2) and (3). Consequently, the observed E_P value depends on whether surface properties of samples were correctly taken into account in determining ε_2 from SE measurements.

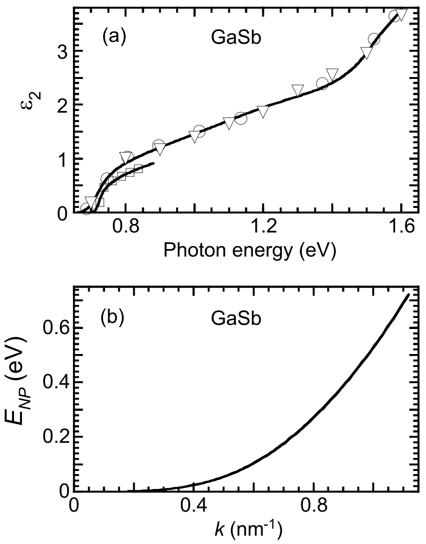

FIG. 15. (top) Fits (solid lines) to ε_2 data for GaSb from Refs. 42 and 111 (circles and triangles, respectively) and from Ref. 112 (squares). The fits result in different E_P values (see text) but the same conduction-band nonparabolicity presented in (bottom) of the figure.

From the above, it follows that our method provides a unique possibility to check the reliability of experimental ε_2 data, as well as to conclude about the value of E_P which would be consistent with the **kp** theory. In particular, we see that the magnitude of ε_2 for GaSb, ZnTe, ZnS, and CdSe is overestimated in existing literature data, probably due to the neglect or incorrect treatment of possible overlayers. Further studies are needed to establish the DF of these compounds in a spectral range close to the absorption edge.

Finally, we briefly discuss a simple model of the CB structure given by Eq. (10). It is clear from the inset of Fig. 2 that an attempt to fit the determined CB dispersion relation by this equation will yield a value of E^* which depends quite strongly on the range of wave vectors to be considered. Comparison of fits by Eqs. (10) and (18) shows that, in general, the latter provides a better description of the CB dispersion relation over a whole range of electron energies. However, the advantage of Eq. (10) is that the quantity E^* can immediately be interpreted as a measure of the nonparabolicity. For example, $E^*=\infty$ would imply a parabolic band, while decreasing E^* corresponds to increasing nonparabolicity. In Table VIII, E^* values are presented, which were obtained in a way that Eq. (10) matches the determined CB dispersion relation at $k=k_0$, where the wave vector k_0 corresponds to an electron concentration $n_e=2\times10^{19}$ cm^{-3}. In Fig. 16, the same data are shown with dependence on the band gap energy (circles and squares for III-V and II-VI semiconductors, respectively). The solid straight line is calculated from $E^*=0.93E_g$. A general trend is that the nonparabolicity scales approximately proportional to E_g, a fact

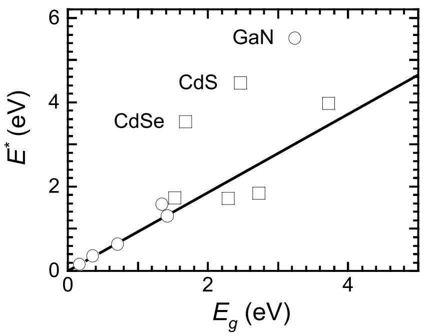

FIG. 16. E^* values at $k=k_0$ [see Eq. (10) and text] with dependence on the band gap energy for III-V (circles) and II-VI (squares) semiconductors (see also Table VIII). The solid line ($E^*=0.93E_g$) is a linear fit to the data points excluding those for GaN, CdSe, and CdS.

generally understood on the basis of Kane's theory. It is interesting to remark that three semiconductors (GaN, CdSe, and CdS), for which the zinc-blende crystal structure is a metastable one, deviate from the general trend toward the side of lower nonparabolicity.

VI. SUMMARY

In the present work, the conduction-band dispersion relation was determined by a comparison of the calculated and experimental imaginary part ε_2 of the dielectric function in a spectral region close to and above the fundamental absorption edge. Investigating GaAs and InP, which served as model materials, we observed that differences between sets of Luttinger parameters proposed by various authors have little effect on the determined dispersion relation for the conduction band. It allows a composite set to be introduced to analyze experimental ε_2 spectra. In this work, we deduced composite Luttinger parameter sets for GaN and II-VI semiconductors based on available literature data. Adjusting calculated ε_2 spectra to experimental ones, we determined the conduction-band dispersion relation for 12 III-V and II-VI zinc-blende semiconductors and deduced the corresponding nonparabolicity coefficients. This yielded an experimental determination of the conduction-band nonparabolicity and effective mass. The results were compared to those available in the literature from experiments and calculations and found to be in very good agreement. With the exception of small-gap semiconductors InSb and InAs, we presented experimental data for the electron momentum effective mass with dependence on the wave vector and free electron concentration, as well as the conduction-band dispersion relation and nonparabolicity extended to electron energies between 0.6 and 2.2 eV depending on the semiconductor of interest, which are significantly higher than those achievable by doping or in magnetic fields.

The results obtained were also analyzed in terms of correspondence to models of the conduction-band structure based on the **kp** theory. We observed that a simple model with only one adjusted parameter provides a good description of the determined conduction-band dispersion relations, especially for GaAs and ZnSe. There are, however, systematic deviations from experimental data, which become more pronounced if a larger wave-vector range is considered, as, e.g., in the case of wide band gap semiconductors. In addition, examining experimental ε_2 data reported by various authors, we were able to conclude that the magnitude of ε_2 for GaSb, ZnTe, ZnS, and CdSe is overestimated in the existing literature data, probably due to the neglect or incorrect treatment of possible overlayers.

ACKNOWLEDGMENT

This work was partially supported by the Deutsche Forschungsgemeinschaft (Grants No. GO 586/6-1 and No. AM 105/5-1).

---

*Corresponding author; sviatoslav.shokhovets@tu-ilmenau.de

[1] E. O. Kane, J. Phys. Chem. Solids **1**, 249 (1957).

[2] W. Zawadzki, Adv. Phys. **23**, 435 (1974).

[3] I. Vurgaftman, J. R. Meyer, and L. R. Ram-Mohan, J. Appl. Phys. **89**, 5815 (2001).

[4] B. K. Meyer and D. M. Hofmann, Phys. Status Solidi B **202**, 783 (1997).

[5] Y. Imanaka, T. Takamusu, K. Takehana, M. Oshikiri, G. Kido, H. Nojiri, Y. H. Matsuda, H. Arimoto, S. Takeyama, N. Miura, G. Karczewski, and T. Wojtowicz, Phys. Status Solidi B **243**, 939 (2006).

[6] *Numerical Data and Functional relationships in Science and Technology*, edited by O. Madelung, M. Schulz, H. Weiss, and U. Rössler, Landolt-Börnstein, New Series, Group III, Vol. 17, Pt. A, (Springer, Berlin, 1982); Vol. 22, Pt. A (Springer, Berlin, 1987); Vol. 41, Pt. A1 (Springer, Berlin, 2002).

[7] *Numerical Data and Functional relationships in Science and Technology*, edited by O. Madelung, U. Rössler, and M. Schulz, Landolt-Börnstein, New Series, Group III, Vol. 41, Pt. B (Springer, Berlin, 1999).

[8] V. B. Golubev, V. I. Ivanov-Omskii, I. G. Minervin, A. V. Osutin, and D. G. Polyakov, Sov. Phys. JETP **61**, 1214 (1985).

[9] H. Sigg, J. A. A. J. Perenboom, P. Pfeffer, and W. Zawadzki, Solid State Commun. **61**, 685 (1987).

[10] M. A. Hopkins, R. J. Nicholas, P. Pfeffer, W. Zawadzki, D. Gauthier, J. C. Portal, and M. A. DiForte-Poisson, Semicond. Sci. Technol. **2**, 568 (1987).

[11] M. Drechsler, P. Emanuelsson, B. K. Meyer, H. Mayer, U. Rössler, and B. Clerjaud, Phys. Rev. B **50**, 2649 (1994).

[12] A. Raymond, J. L. Robert, and C. Bernard, J. Phys. C **12**, 2289 (1979).

[13] D. Schneider, D. Rürup, A. Plichta, H.-U. Grubert, A. Schlachetzki, and K. Hansen, Z. Phys. B: Condens. Matter **95**, 281 (1994).

[14] G. Ambrazevičius, M. Cardona, and R. Merlin, Phys. Rev. Lett. **59**, 700 (1987).

[15] T. Ruf and M. Cardona, Phys. Rev. B **41**, 10747 (1990).

[16] U. Rössler, Solid State Commun. **49**, 943 (1984).

[17] (a) P. Pfeffer and W. Zawadzki, Phys. Rev. B **41**, 1561 (1990); (b) **53**, 12813 (1996).

[18] A. N. Chantis, M. van Schilfgaarde, and T. Kotani, Phys. Rev. Lett. **96**, 086405 (2006).

[19] S. Shokhovets, G. Gobsch, and O. Ambacher, Appl. Phys. Lett. **86**, 161908 (2005); Superlattices Microstruct. **39**, 299 (2006).

[20] S. Shokhovets, G. Gobsch, and O. Ambacher, Phys. Rev. B **74**, 155209 (2006).

[21] S. Zollner, J. Appl. Phys. **90**, 515 (2001).

[22] C. M. Herzinger, P. G. Snyder, B. Johs, and J. A. Woollam, J. Appl. Phys. **77**, 1715 (1995).

[23] A. Baldereschi and N. C. Lipari, Phys. Rev. B **8**, 2697 (1973).

[24] S. L. Chuang, *Physics of Optoelectronic Devices* (Wiley, New York, 1995), Chap. 13.

[25] H. Fu, L.-W. Wang, and A. Zunger, Phys. Rev. B **57**, 9971 (1998).

[26] M. Suzuki and T. Uenoyama, Appl. Phys. Lett. **69**, 3378 (1996).

[27] W. J. Fan, M. F. Li, T. C. Chong, and J. B. Xia, J. Appl. Phys. **79**, 188 (1996).

[28] D. Ahn, J. Appl. Phys. **79**, 7731 (1996).

[29] J.-B. Xia, K. W. Cheah, X.-L. Wang, D.-Z. Sun, and M.-Y. Kong, Phys. Rev. B **59**, 10119 (1999).

[30] S.-H. Park and S. L. Chuang, J. Appl. Phys. **87**, 353 (2000).

[31] S. K. Pugh, D. J. Dugdale, S. Brandt, and R. A. Abram, Semicond. Sci. Technol. **14**, 23 (1999).

[32] L. E. Ramos, L. K. Teles, L. M. R. Scolfaro, J. L. P. Castineira, A. L. Rosa, and J. R. Leite, Phys. Rev. B **63**, 165210 (2001).

[33] D. Fritsch, H. Schmidt, and M. Grundmann, Phys. Rev. B **67**, 235205 (2003).

[34] P. Rinke, M. Scheffler, A. Qteish, M. Winkelnkemper, D. Bimberg, and J. Neugebauer, Appl. Phys. Lett. **89**, 161919 (2006).

[35] M. Fanciulli, T. Lei, and T. D. Moustakas, Phys. Rev. B **48**, 15144 (1993).

[36] K. Miwa and A. Fukumoto, Phys. Rev. B **48**, 7897 (1993).

[37] W. W. Chow, A. F. Wright, and J. S. Nelson, Appl. Phys. Lett. **68**, 296 (1996).

[38] M. Städele, M. Moukara, J. A. Majewski, P. Vogl, and A. Görling, Phys. Rev. B **59**, 10031 (1999).

[39] A. V. Rodina, M. Dietrich, A. Göldner, L. Eckey, A. Hoffmann, Al. L. Efros, M. Rosen, and B. K. Meyer, Phys. Rev. B **64**, 115204 (2001).

[40] H.-R. Trebin and U. Rössler, Phys. Status Solidi B **70**, 717 (1975); H.-R. Trebin, *ibid.* **81**, 527 (1977).

[41] U. Köhler, D. J. As, B. Schöttker, T. Frey, K. Lischka, J. Scheiner, S. Shokhovets, and R. Goldhahn, J. Appl. Phys. **85**, 404 (1999); S. S. is indebted to D. J. As for providing epitaxial layers of cubic GaN to extend the previous experimental data for the DF up to 5.5 eV.

[42] M. Muñoz, K. Wei, F. H. Pollak, J. L. Freeouf, and G. W. Charache, Phys. Rev. B **60**, 8105 (1999).

[43] S. Adachi, *Optical Constants of Crystalline and Amorphous Semiconductors: Numerical Data and Graphical Information* (Kluwer Academic, Boston, 1999).

[44] E. Otsuka, in *Landau Level Spectroscopy*, edited by G. Landwehr and E. I. Rashba (North-Holland, Amsterdam, 1991), Chap. 1; D. G. Seiler and A. E. Stephens, *ibid.*, Chap. 18.

[45] D. G. Seiler and W. M. Becker, Phys. Rev. **183**, 784 (1969).

[46] C. Alibert, A. Joullié, A. M. Joullié, and C. Ance, Phys. Rev. B **27**, 4946 (1983).

[47] H. Arimoto, N. Miura, R. J. Nicholas, N. J. Mason, and P. J. Walker, Phys. Rev. B **58**, 4560 (1998).

[48] C. Ghezzi, R. Magnanini, A. Parisini, B. Rotelli, L. Tarricone, A. Bosacchi, and S. Franchi, Phys. Rev. B **52**, 1463 (1995).

[49] G. N. Aliev, N. P. Gavaleshko, O. S. Koshug, V. I. Pleshko, R. P. Seisyan, and K. D. Sushkevich, Sov. Phys. Solid State **34**, 1286 (1992).

[50] S. Lee, F. Michl, U. Rössler, M. Dobrowolska, and J. K. Furdyna, Phys. Rev. B **57**, 9695 (1998).

[51] A. Mang, K. Reimann, St. Rübenacke, and M. Steube, Phys. Rev. B **53**, 16283 (1996).

[52] T. Taguchi, T. Yokogawa, and H. Yamashita, Solid State Commun. **49**, 551 (1984).

[53] G. N. Aliev, O. S. Coshug, A. I. Nesvizskii, R. P. Seisyan, and T. V. Yazeva, Phys. Solid State **35**, 764 (1993).

[54] R. H. Lyddane, R. G. Sachs, and E. Teller, Phys. Rev. **59**, 673 (1941).

[55] D. T. F. Marple, J. Appl. Phys. **35**, 539 (1964).

[56] W. L. Bond, J. Appl. Phys. **36**, 1674 (1965).

[57] A. N. Pikhtin and A. D. Yaskov, Fiz. Tekh. Poluprovodn. (S. Peterburg) **12**, 1047 (1978).

[58] R. Geick, C. H. Perry, and S. S. Mitra, J. Appl. Phys. **37**, 1994 (1966).

[59] H. W. Verleur and A. S. Barker, Jr., Phys. Rev. **155**, 750 (1967).

[60] A. S. Barker, Jr. and C. J. Summers, J. Appl. Phys. **41**, 3552 (1970).

[61] J. Serrano, A. Cantarero, M. Cardona, N. Garro, R. Lauck, R. E. Tallman, T. M. Ritter, and B. A. Weinstein, Phys. Rev. B **69**, 014301 (2004).

[62] M. Schall, M. Walther, and P. U. Jepsen, Phys. Rev. B **64**, 094301 (2001).

[63] I. Strzalkowski, S. Joshi, and C. R. Crowell, Appl. Phys. Lett. **28**, 350 (1976).

[64] I. B. Kobyakov and G. S. Pado, Sov. Phys. Solid State **9**, 1707 (1968).

[65] I. B. Kobyakov, Solid State Commun. **35**, 305 (1980).

[66] G. A. Samara, Phys. Rev. B **27**, 3494 (1983).

[67] G. Gallot, J. Zhang, R. W. McGowan, T.-I. Jeon, and D. Grischkowsky, Appl. Phys. Lett. **74**, 3450 (1999).

[68] L. Thamizhmani, A. K. Azad, J. Dai, and W. Zhang, Appl. Phys. Lett. **86**, 131111 (2005).

[69] R. A. Stradling, Solid State Commun. **6**, 665 (1968).

[70] P. Lawaetz, Phys. Rev. B **4**, 3460 (1971).

[71] S. Nakashima, T. Hattori, P. E. Simmonds, and E. Amzallag, Phys. Rev. B **19**, 3045 (1979).

[72] H. Venghaus and B. Jusserand, Phys. Rev. B **22**, 932 (1980).

[73] Y. Oka and M. Cardona, Phys. Rev. B **23**, 4129 (1981).

[74] W. Maier, G. Schmieder, and C. Klingshirn, Z. Phys. B: Condens. Matter **50**, 193 (1983).

[75] C. Neumann, A. Nöthe, and N. O. Lipari, Phys. Rev. B **37**, 922 (1988).

[76] M. Said and M. A. Kanehisa, Phys. Status Solidi B **157**, 311 (1990).

[77] H. P. Wagner, S. Lankes, K. Wolf, D. Lichtenberg, W. Kuhn, P. Link, and W. Gebhardt, J. Lumin. **52**, 41 (1992).

[78] M. Sondergeld, Phys. Status Solidi B **81**, 4637 (1977).

[79] S. Feierabend and G. Weber, Solid State Commun. **26**, 253 (1978).

[80] H. Venghaus, Phys. Rev. B **19**, 3071 (1979).

[81] B. Sermage and G. Fishman, Phys. Rev. B **23**, 5107 (1981).

[82] U. Rössler and H.-R. Trebin, Phys. Rev. B **23**, 1961 (1981).

[83] H. W. Hölscher, A. Nöthe, and Ch. Uihlein, Phys. Rev. B **31**, 2379 (1985).

[84] S. Lankes, M. Meier, T. Reisinger, and W. Gebhardt, J. Appl. Phys. **80**, 4049 (1996).

[85] H. Nakata, K. Yamada, and T. Ohyama, Phys. Rev. B **60**, 13269 (1999).

[86] L. Svob, Y. Marfaing, M. Hoclet, P. Plumelle, and M. Vandevyver, Solid State Commun. **28**, 895 (1978).

[87] L. S. Dang, G. Neu, and R. Romestain, Solid State Commun. **44**, 1187 (1982).

[88] T. Fridrich, J. Kraus, M. Meininger, G. Schaack, and W. O. G. Schmitt, J. Phys.: Condens. Matter **6**, 4307 (1994).

[89] A. I. Ekimov, F. Hache, M. C. Schanne-Klein, D. Richard, C. Flytzanis, I. A. Kudryavtsev, T. V. Yazeva, A. V. Rodina, and Al. L. Efros, J. Opt. Soc. Am. B **10**, 100 (1993).

[90] D. J. Norris and M. G. Bawendi, Phys. Rev. B **53**, 16338 (1996).

[91] T. Richard, P. Lefebvre, H. Mathieu, and J. Allègre, Phys. Rev. B **53**, 7287 (1996).

[92] J.-B. Jeon, Y. M. Sirenko, K. W. Kim, M. A. Littlejohn, and M. A. Stroscio, Solid State Commun. **99**, 423 (1996).

[93] Al. L. Efros and M. Rosen, Phys. Rev. B **58**, 7120 (1998).

[94] E. P. Pokatilov, V. A. Fonoberov, V. M. Fomin, and J. T. Devreese, Phys. Rev. B **64**, 245328 (2001).

[95] V. A. Fonoberov, E. P. Pokatilov, and A. A. Balandin, Phys. Rev. B **66**, 085310 (2002).

[96] D. O. Demchenko and L.-W. Wang, Phys. Rev. B **73**, 155326 (2006).

[97] F. C. Peiris, B. A. Kowalski, X. Liu, U. Bindley, and J. K. Furdyna, J. Appl. Phys. **94**, 4717 (2003).

[98] M. S. Koo, T. J. Kim, M. S. Lee, M. S. Oh, Y. D. Kim, S. D. Yoo, D. E. Aspnes, and B. T. Jonker, Appl. Phys. Lett. **77**, 3364 (2000).

[99] S. Ozaki and S. Adachi, Jpn. J. Appl. Phys., Part 1 **32**, 5008 (1993).

[100] C. C. Kim, M. Daraselia, J. W. Garland, and S. Sivananthan, Phys. Rev. B **56**, 4786 (1997).

[101] Y. D. Kim, M. V. Klein, S. F. Ren, Y. C. Chang, H. Luo, N. Samarth, and J. K. Furdyna, Phys. Rev. B **49**, 7262 (1994).

[102] U. Rossow, T. Werninghaus, D. R. T. Zahn, W. Richter, and K. Horn, Thin Solid Films **233**, 176 (1993); see also Ref. 42.

[103] J. Kvietkova, B. Daniel, M. Hetterich, M. Schubert, D. Spemann, D. Litvinov, and D. Gerthsen, Phys. Rev. B **70**, 045316 (2004).

[104] T. Ohyama, K. Sakakibara, E. Otsuka, M. Isshiki, and K. Igaki, Phys. Rev. B **37**, 6153 (1988).

[105] Y. Imanaka, N. Miura, and H. Kukimoto, Phys. Rev. B **49**, 16965 (1994).

[106] H. Mayer and U. Rössler, Solid State Commun. **87**, 81 (1993).

[107] D. T. F. Marple, J. Appl. Phys. **35**, 1879 (1964).

[108] K. C. Agarwal, B. Daniel, M. Grün, P. Feinäugle, C. Klingshirn, and M. Hetterich, Appl. Phys. Lett. **86**, 181907 (2005).

[109] C. Hermann and C. Weisbuch, Phys. Rev. B **15**, 823 (1977).

[110] M. Muñoz, Y. S. Huang, F. H. Pollak, and H. Yang, J. Appl. Phys. **93**, 2549 (2003).

[111] R. Ferrini, M. Patrini, and S. Franchi, Appl. Phys. Lett. **84**, 4517 (1998).

[112] Reference 48; see also Ref. 43.

[113] K. Sato and S. Adachi, J. Appl. Phys. **73**, 926 (1993).

[114] C. C. Kim and S. Sivananthan, Phys. Rev. B **53**, 1475 (1996).

[115] S. Adachi and T. Taguchi, Phys. Rev. B **43**, 9569 (1991).

[116] H. Arwin and D. E. Aspnes, J. Vac. Sci. Technol. A **2**, 1316 (1984).

[117] Q. H. F. Vrehen, J. Phys. Chem. Solids **29**, 129 (1968).

[118] I. Balslev, Phys. Rev. **177**, 1173 (1969).

[119] R. P. Seisyan, M. A. Abdullaev, and V. D. Drazin, Sov. Phys. Semicond. **7**, 522 (1973).

[120] M. S. Skolnick, A. K. Jain, R. A. Stradling, J. Leotin, J. C. Ousset, and S. Askenazy, J. Phys. C **9**, 2809 (1976).

[121] D. Bimberg, in *Advances in Solid State Physics*, edited by J. Treusch (Vieweg, Braunschweig, 1977), Vol. XVII, p. 195.

[122] W. Ekardt, K. Lösch, and D. Bimberg, Phys. Rev. B **20**, 3303 (1979).

[123] R. Eppenga, M. F. H. Schuurmans, and S. Colak, Phys. Rev. B **36**, 1554 (1987).

[124] L. W. Molenkamp, R. Eppenga, G. W.'t Hooft, P. Dawson, C. T. Foxon, and K. J. Moore, Phys. Rev. B **38**, 4314 (1988).

[125] B. V. Shanabrook, O. J. Glembocki, D. A. Broido, and W. I. Wang, Phys. Rev. B **39**, 3411 (1989).

[126] N. Binggeli and A. Baldereschi, Phys. Rev. B **43**, 14734 (1991).

[127] T. E. Ostromek, Phys. Rev. B **54**, 14467 (1996).

[128] S. Richard, F. Aniel, and G. Fishman, Phys. Rev. B **70**, 235204 (2004).

[129] R. L. Bowers and G. D. Mahan, Phys. Rev. **185**, 1073 (1969).

[130] J. Leotin, R. Barbaste, S. Askenazy, M. S. Skolnick, R. A. Stradling, and J. Tuchendler, Solid State Commun. **15**, 693 (1974).

[131] P. Rochon and E. Fortin, Phys. Rev. B **12**, 5803 (1975).

[132] D. Bimberg, K. Hess, N. O. Lipari, J. U. Fischbach, and M. Altarelli, Physica B **81**, 139 (1977).

[133] Y. Chen, B. Gil, H. Mathieu, and J. P. Lascaray, Phys. Rev. B **36**, 1510 (1987).

[134] M. Cardona, N. E. Christensen, and G. Fasol, Phys. Rev. B **38**, 1806 (1988).

[135] C. W. Litton, R. B. Dennis, and S. D. Smith, J. Phys. C **2**, 2146 (1969).

[136] J. M. Chamberlain, P. E. Simmonds, and R. A. Stradling, J. Phys. C **4**, L38 (1971).

[137] G. Lindemann, R. Lassnig, W. Seidenbusch, and E. Gornik, Phys. Rev. B **28**, 4693 (1983).

[138] N. Ahmed, I. R. Agool, M. G. Wright, K. Mitchell, A. Koohian, S. J. A. Adams, C. R. Pidgeon, B. C. Cavenett, C. R. Stanley, and A. H. Kean, Semicond. Sci. Technol. **7**, 357 (1992).

[139] J. G. Michels, R. J. Warburton, R. J. Nicolas, and C. R. Stanley, Semicond. Sci. Technol. **9**, 198 (1994).

[140] E. P. Rashevskaya, V. I. Fistul, and M. G. Milvidskii, Fiz. Tverd. Tela (Leningrad) **8**, 3135 (1966).

[141] H. R. Chandrasekhar and A. K. Ramdas, Phys. Rev. B **21**, 1511 (1980).

[142] Y. I. Ukhanov, Fiz. Tverd. Tela (Leningrad) **5**, 108 (1963).

[143] T. Ohyama, E. Otsuka, S. Yamada, T. Fukui, and N. Kobayashi, Jpn. J. Appl. Phys., Part 2 **22**, L742 (1983).

[144] M. Helm, W. Knap, W. Seidenbusch, R. Lassnig, E. Gornik, R. Triboulet, and L. L. Taylor, Solid State Commun. **53**, 547 (1985).

[145] A. Moll, C. Wetzel, B. K. Meyer, P. Omling, and F. Scholz, Phys. Rev. B **45**, 1504 (1992).

[146] S. Askenazy, R. Barbaste, J. Leotin, J. C. Portal, J. P. Ulmet, J. M. Chamberlain, and R. A. Stradling, Solid State Commun. **9**, 729 (1971).

[147] F. P. Kesamanly, D. N. Nasledov, A. Y. Nashelskii, and V. A.

Skripkin, Fiz. Tekh. Poluprovodn. (S.-Peterburg) **2**, 1463 (1968).

[148] F. Köhl, J. Phys. Chem. Solids **32**, 2481 (1971).

[149] W. K. Metzger, M. W. Wanlass, L. M. Gedvilas, J. C. Verley, J. J. Caparella, and R. K. Ahrenkiel, J. Appl. Phys. **92**, 3524 (2002).

[150] B. Clerjaud, A. Gelineau, D. Galland, and K. Saminadayar, Phys. Rev. B **19**, 2056 (1979).

[151] P. J. Dean, H. Venghaus, and P. E. Simmonds, Phys. Rev. B **18**, 6813 (1978).

[152] Y. Imanaka and N. Miura, Phys. Rev. B **50**, 14065 (1994).

[153] K. K. Kanazawa and F. C. Brown, Phys. Rev. **135**, A1757 (1964).

[154] A. L. Mears and R. A. Stradling, Solid State Commun. **7**, 1267 (1969).

[155] J. Waldman, D. M. Larsen, P. E. Tannenwald, C. C. Bradley, D. R. Cohn, and B. Lax, Phys. Rev. Lett. **23**, 1033 (1969).

[156] P. E. Simmonds, J. M. Chamberlain, R. A. Hoult, R. A. Stradling, and C. C. Bradley, J. Phys. C **7**, 4164 (1974).

[157] D. T. F. Marple, Phys. Rev. **129**, 2466 (1963).